CHEMISTRY OF MATERIALS
ARTICLE
pubs.acs.org/cm

Atomic Layer Deposition of Ruthenium Using the Novel Precursor bis(2,6,6-trimethyl-cyclohexadienyl)ruthenium

Keith Gregorczyk,[†] Laurent Henn-Lecordier,[◆,†] Julien Gatineau,[‡] Christian Dussarrat,[§] and Gary Rubloff[*,†]

[†]Department of Material Science and Engineering & Institute for Systems Research, University of Maryland, College Park, Maryland 20742, United States

[‡]Air Liquide Laboratoires, Tsukuba, Ibaraki, 300-4247 Japan

[§]Air Liquide, DRTC, 200 GBC Drive, Newark, Delaware 19402, United States

ABSTRACT: A recently reported ruthenium molecule, bis(2,6,6-trimethyl-cyclohexadienyl)-ruthenium, has been developed and characterized as a precursor for atomic layer deposition (ALD) of ruthenium. This molecule, which has never been reported as an ALD precursor, was developed to address low growth rates, high nucleation barriers, and undesirable precursor phases commonly associated with other Ru precursors such as RuCp and Ru(EtCp)$_2$. The newly developed precursor has similar vapor pressure to both RuCp and Ru(EtCp)$_2$ but offers significant improvement in stability as evaluated by thermogravimetric analysis and differential scanning calorimetry. In an ALD process, it provides good self-limiting growth, with a 0.5 Å/cycle growth rate under saturated dose conditions in a temperature between 250 and 300 °C. Furthermore, the precursor exhibits considerably better nucleation characteristics on SiO$_2$, TiO$_2$, and H-terminated Si surfaces, compared to RuCp$_2$ and Ru(EtCp)$_2$.

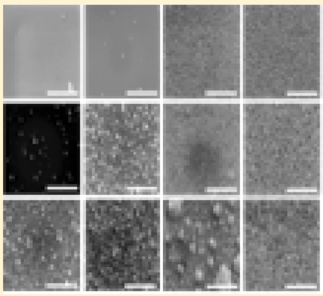

KEYWORDS: atomic layer deposition, ruthenium, thin film

INTRODUCTION

Atomic layer deposition (ALD) is based on a sequence of self-limited chemisorbed surface reactions that confers unprecedented thickness control at the atomic level, excellent across-wafer uniformity, and unmatched conformality over the most stringent 3D structures.[1] As a result, the range of ALD applications has rapidly expanded beyond logic and memory devices and is now permeating fields as varied as optoelectronics, catalysis, energy, and biomaterials.[2]

The selection of precursors to deposit oxide materials is broad, including a large variety of metal oxides, mixed alloys, and laminates of these oxides, typically with several precursor choices available for the metal−organic component. ALD precursors and processes for single-element metal films is more limited, including molybdenum,[3] tungsten,[4−7] copper,[8,9] iron, cobalt, nickel,[9] platinum,[10] palladium,[11,12] rhodium,[13] and iridium.[14] In many cases, these processes suffer from problems that hinder their practical application, such as low-vapor-pressure precursors, lower growth rates, delayed or slow nucleation, and highly corrosive halide byproduct (e.g., HF or HCl).

Within single-element metals, ruthenium is of particular interest, because of its high work function (4.7 eV), low bulk resistivity (7 $\mu\Omega$ cm), and, for some applications, its conducting oxide phase (RuO$_2$). These electrodes are used in high-aspect-ratio random access memory devices (e.g., dynamic RAM,[15−18] ferroelectric RAM,[17] or magnetic RAM[19]), gate metal in MOSFETs,[20] a glue layer for CVD-grown and electrodeposited copper films,[21,22] and gas-sensing nanostructures.[23] Ru has also been shown to force TiO$_2$ films grown on it into the high-*K* rutile phase, making it attractive for capacitor applications.[24]

The most commonly used Ru ALD precursors belong to the cyclopentadienyl class, which include RuCp$_2$,[25] and Ru(EtCp)$_2$.[21,26] Although both have reasonable growth rates per cycle (GPC) (i.e., 0.45 and 1.5 Å/cycle respectively), large nucleation barriers on the order of several hundred cycles have been reported (i.e., the GPC is either slow or delayed in reaching a steady state value, as a function of ALD cycle number). This limits the ability to accurately control the film thickness, while leading to a waste of expensive precursor. The next most common class of Ru precursors—the tris-β-diketonates, which includes Ru(thd)$_3$[27,28]—are solid at room temperature (with the exception of Ru(Od)$_3$[29]) and, therefore, present additional challenges regarding reactant delivery, because of their inherently low vapor pressure. Growth rates reported by Aaltonen et al.[27] when using Ru(thd)$_3$ in its solid form were the lowest reported growth rates of all the Ru precursors (0.36 Å/cycle).[27] Kim et al. dissolved the solid precursor in ethylcyclohexane in order to use a liquid injection system.[28] While self-limiting growth was achieved, the growth per cycle was dependent on both the concentration of Ru(thd)$_3$ solution in ethylcyclohexane and flow rate of the delivery gas through the liquid injection system. Even in this case, the GPC value was not improved, with a reported value of ~0.3 Å /cycle.[28] A higher GPC (i.e., 0.8 Å /cycle) was achieved over a 325−375 °C temperature window in the case of Ru(Od)$_3$, although a liquid injection system was still required, presumably because of its low vapor pressure. Ru(IPMB)-(CHD), which is a custom-made precursor, was reported and showed an excellent growth rate, compared to Cp-based chemistries, high uniformity and conformality, and slow nucleation.[30]

Received: February 15, 2011
Revised: April 7, 2011
Published: April 27, 2011

However, the temperature window was not reported, and, because of the complicated synthesis, this precursor does not seem to be readily available. *N*,*N*-RuCp was investigated as a high-temperature precursor and showed a saturated growth rate of 0.5 Å /cycle between 400 °C and 450 °C. Additional precursors that require oxygen or ammonia plasma to promote nucleation were also reported, although such processes can potentially induce substrate damage from the reactive ions.

Despite the large amount of work done to develop an ALD process for ruthenium, the same basic problems still exist, namely, large nucleation delays on many substrates and relatively low growth rates. An ideal ALD process should have a GPC of ~1 Å/cycle (which is consistent with a single monolayer of the deposited material) and a short nucleation delay (on the order of ~10 cycles or less). In most prior reports, improvement on one of these parameters (i.e., reactivity as GPC or nucleation rate) leads to a marked loss in the other (i.e., stability), or the authors report an improved property without reference to other important parameters.

In this paper, we report the development and application of a novel ruthenium precursor, bis(2,6,6-trimethyl-cyclohexadienyl)ruthenium for noble metal ALD deposition. A recently reported molecule was developed as an ALD Ru precursor to circumvent issues generated by commonly used molecules studied in the literature, such as $RuCp_2$ and $Ru(EtCp)_2$.[31] We have developed an ALD process for the new precursor and report self-limiting growth, ALD kinetics, and film characterization by XRD and SEM. This new precursor's key characteristics can be summarized as follows:

- stable in air,
- liquid (at room temperature) with a high enough vapor pressure to circumvent the need for a liquid injection system or solvent dissolution,
- growth rates similar to the Cp family with significantly shorter nucleation delays on most substrates,
- a stable ALD temperature process window, and
- phase transition from Ru to RuO_2 at higher O_2 partial pressure.

EXPERIMENT

$Ru(C_9H_{13})_2$ (or "Cyprus") is a new, commercially available, and proprietary molecule prepared and characterized by Air Liquide as new precursor for ALD. Thermal analysis of $Ru(C_9H_{13})_2$ was conducted in two ways and compared to $Ru(EtCp)_2$. Thermogravimetric measurements were performed using a Mettler-Toledo model STARe TG/SDTA851e system with samples in an inert atmosphere (O_2 and H_2O <5 ppm). Both samples were heated at a rate of 10 °C/min, and these data were used to calculate the vapor pressure of $Ru(C_9H_{13})_2$ and $Ru(EtCp)_2$, while the vapor pressure for $RuCp_2$ was taken from the literature.[32] Differential scanning calorimetry (DSC) experiments were performed using a Bruker model DSC3300 system with a heating rate of 10 °C/min as well. All samples were prepared under an inert atmosphere (O_2 and H_2O <5 ppm). Stability of the $Ru(C_9H_{13})_2$ was observed visually: after exposure to air, no color change or temperature change was noticed, which indicated that no reaction had occurred.

Ruthenium deposition experiments were conducted in a wafer-scale cross-flow ALD reactor. This load-locked system houses a 0.2-L reaction chamber operating in the 0.1−1 Torr pressure regime, the relatively small chamber volume being conducive to subsecond residence times. The system features a single-wafer substrate heater, which was calibrated using a SensArray wafer instrumented with 13 thermocouples. Details on the design and operation of this system are discussed in previously published work.[6,7]

Research-grade oxygen (Praxair, 99.999% purity) was delivered through a needle valve and timed Swagelok ALD valve. The Ru precursor was loaded in a Strem electropolished stainless-steel bubbler maintained at 60 °C. Using a three way-valve, 10 sccm N_2 was flowed through the bubbler, with the dose being regulated by the actuation time of a downstream ALD valve.

All the experiments were conducted on 4-in. (100 mm) Si(100) wafers. Silicon wafers were dipped in a 3% HF solution for 20 s, followed by a deionized (DI) water rinse and blow drying with N_2 prior to being transferred to the load-lock.

To test the ALD growth properties of the $Ru(C_9H_{13})_2$ precursor on different materials, films of SiO_2, TiO_2, and Al_2O_3 were first grown on the wafers. 110-nm SiO_2 films were grown by CVD in a Tystar CVD system. TiO_2 and Al_2O_3 films (25 nm thick) were deposited in a commercial Beneq TFS500 ALD reactor, using water as an oxidant and tetrakisdimethylamido titanium (TDMAT) and trimethyl aluminum (TMA), respectively, as metal organic precursors.

Process optimization experiments were conducted exclusively on the SiO_2 coated wafers. Each run consisted of 300 cycles of deposition, unless otherwise noted. Under optimized process conditions, a cycle sequence consisted of a 5 s $Ru(C_9H_{13})_2$ pulse, a 15 s pumpdown/purge to return the chamber back to base pressure, a 1 s O_2 pulse at 1.2 Torr, and a final 15 s pumpdown.

Film thicknesses were measured ex situ with a Sopra GES5 spectroscopic ellipsometer. Thickness profiles for each wafer, unless otherwise noted, were mapped by measuring a 25-point grid. The average thickness of these points is reported as the thickness and the nonuniformity was estimated from the ratio of the standard deviation of the 25 points divided by the mean. The structure of the films were examined by SEM, using a Hitachi model SU-70 Analytical UHR FEG system and a Bruker model D8 Discover Powder Diffractometer using Cu Kα radiation and equipped with a Göbel mirror and HiStar area detector to study their morphology and crystallinity.

PRECURSOR DEVELOPMENT

In order to address and circumvent issues generated by molecules studied in the literature, bis(2,6,6-trimethyl-cyclohexadienyl)ruthenium ($Ru(C_9H_{13})_2$) was developed as a new commercially available ALD precursor.[31] Because of the proprietary nature of its production, the exact details of its commercial synthesis cannot be revealed, although a more general discussion will help to elucidate its improved performance as an ALD precursor. To understand the properties of this complex, it is informative to discuss the properties of other more common ruthenium complexes. As mentioned in the Introduction, many different Ru complexes that will deposit via ALD are available. The most commonly used, $Ru(EtCp)_2$, was shown to react with O_2 to deposit ruthenium,[21] but it exhibits very large nucleation delays (on the order of several hundred cycles) that limit the potential for industrialization, as was shown in a MOCVD process.[33] In comparison, (2,4-dimethylpentadienyl)-(ethylcyclopentadienyl)ruthenium (called DER) has also been evaluated in prior work. The difference between these two molecules only originates in the substitutions of one ethylcyclopentadienyl ligand by one 2,4-dimethylpentadienyl (DMPD) ligand. As a result, it was reported that depositions with a shorter nucleation delay were possible using DER.[33,34] Unfortunately, by changing this ligand, the same authors[34] noted a marked decrease in the thermal stability, by ~100 °C, as compared to $Ru(EtCp)_2$. This decrease in thermal stability of DER was reported to be due

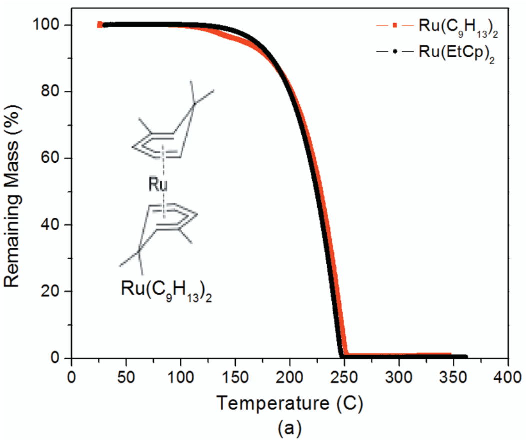

Figure 1. Thermal characterization. (a) Thermogravimetric analysis showing a comparison between Ru(C_9H_{13})$_2$ and commonly used Ru(EtCp)$_2$ (inset shows the chemical structure of Ru(C_9H_{13})$_2$[31]); these data show smooth evaporation with no signs of decomposition below 250 °C. (b) DSC measurements showing thermal breakdown of Ru(C_9H_{13})$_2$, compared to Ru(EtCp)$_2$; peaks clearly corresponding to an exothermic reaction are seen at 375 °C for Ru(EtCp)$_2$ and 425 °C for Ru(C_9H_{13})$_2$, confirming the increase in stability.

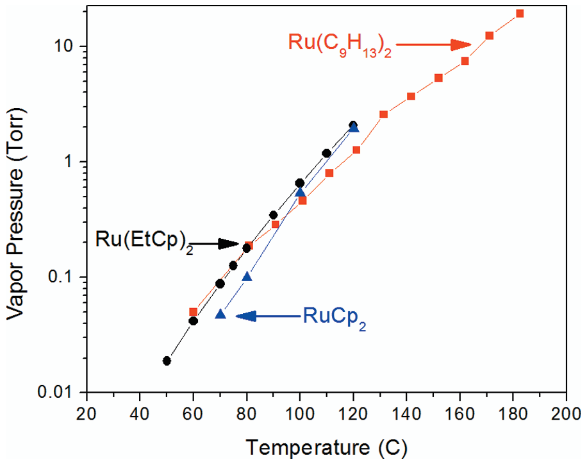

Figure 2. Vapor pressure of Ru(C_9H_{13})$_2$, compared to other Cp complexes, showing a good comparison to commonly used ruthenium precursors.

to the less-stable bonding between the DMPD ligands and the Ru ions.[34] We may conclude that, despite the decrease in the thermal stability, it is desirable to replace cyclopentadienyl ligands with more reactive pentadienyl ligands.[31]

Our experience shows that (2,4-dimethyl-pentadienyl)-(ethylcyclopentadienyl)ruthenium and the related bis(2,4-dimethyl-pentadienyl)ruthenium can only be prepared with low yield from the precursor synthesis process. As a consequence, we considered alternatives to 2,4-dimethylpentadienyl in order to take advantage of the higher reactivity of the outer vinyl carbons. Among them, the cyclohexadienyl structure appears similar to the 2,4-dimethylpentadienyl structure, except for the out-of-plane carbon bridging the outer sp^2 carbons, which can be seen in the inset of Figure 1. The edge-bridged open ruthenocene structure of the cyclohexadienyl ligand and the increased steric bulk make this complex more thermally stable than DER or Ru(EtCp)$_2$, and the closed carbon ring was expected to enhance the reactivity of the molecule with the co-reactant O$_2$. To confirm this, thermogravimetric and DSC measurements were made. Thermogravimetric results for Ru(C_9H_{13})$_2$ is compared to those for Ru(EtCp)$_2$ in Figure 1a, showing that both molecules evaporate smoothly without leaving significant residue. The end-of-evaporation temperatures are very close for both molecules, implying that the molecules have very similar vapor pressures. The absence of residual mass amounts confirms the thermal stability of both molecules, up to 250 °C.

To investigate the behavior of both molecules at higher temperatures, DSC measurements were made as shown in Figure 1b. The decomposition onset, which corresponds to an exothermic reaction, is clearly seen at 375 °C for Ru(EtCp)$_2$, while an onset at 425 °C occurs for Ru(C_9H_{13})$_2$, making it more thermally stable and more reactive with the coreactant O$_2$ than both Ru(EtCp)$_2$ and DER. Furthermore, the new precursor Ru(C_9H_{13})$_2$, bis(2,6,6-trimethyl-cyclohexadienyl)ruthenium, is a liquid at room temperature, is stable in air, and has a similar vapor pressure to Ru(EtCp)$_2$ and RuCp$_2$ (shown in Figure 2), thus making it a suitable candidate for ALD deposition of high-quality Ru films.

■ ALD PROCESS

To characterize the ability of Ru(C_9H_{13})$_2$ to induce self-limited chemisorbed reactions to achieve the benefits of ALD, the metal-organic precursor was used with O$_2$ in an ALD process carried out in the cross-flow reactor. In Figure 3, the surface saturation of Ru(C_9H_{13})$_2$ and O$_2$ precursors was investigated by measuring the GPC as a function of Ru(C_9H_{13})$_2$ pulse time (Figure 3a) and O$_2$ pulse pressure (Figure 3b). The top axis on both figures provides estimations of the corresponding doses in micromoles (μmol), as calculated using a standard bubbler delivery model[35] in the case of Ru(C_9H_{13})$_2$ and an experimental calibration procedure derived from the ideal gas law for the oxygen precursor. In the case of Ru(C_9H_{13})$_2$ pulse time, the growth per cycle (GPC) reaches a plateau at 0.5 Å/cycle for exposure above 3 s (2.2 μmol), as Ru-based adsorbed molecules fully saturate the surface, resulting in a self-limited half-reaction characteristic of ALD.

The effect of reactant depletion in the under exposure regime is clearly in evidence, as revealed by the use of the cross-flow reactor

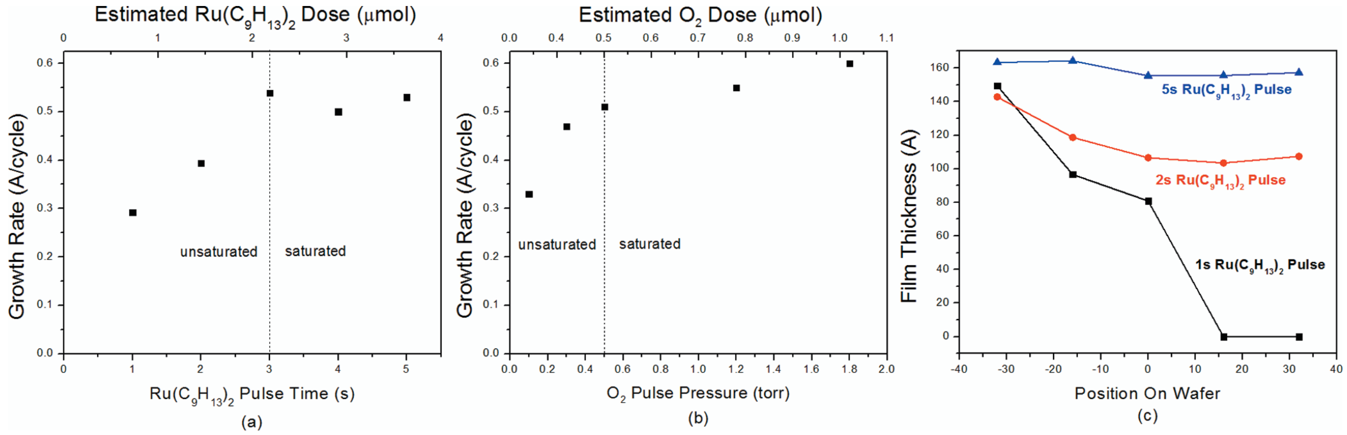

Figure 3. Growth rate of Ru film as a function of (a) Ru(C_9H_{13})$_2$ pulse time and (b) O_2 pulse pressure. While holding the oxygen pulse at 1.2 Torr, the cross-wafer thickness as a function of position on the wafer (panel c) for two points in the unsaturated region and one in the saturated region was studied. The black squares represent measurements made for Ru(C_9H_{13})$_2$ pulse times of 1 s, the red circles for pulse times of 2 s. The blue triangles show fully saturated conditions at pulse times of 5 s.

configuration, as shown in Figure 3c, the film thickness across the wafer drops along the direction of the flow for 1 s (black squares) and 2 s (red circles) Ru(C_9H_{13})$_2$ exposures, clearly indicating an incomplete saturation of the surface sites across the wafer. O_2 pulse time and pressure were held constant at 1 s and 1.2 Torr during these measurements. Saturated ALD dose conditions are seen for 5 s pulses (blue triangles), across-wafer uniformity is greatly improved, with a nonuniformity of <5% on SiO_2 substrates and <2% on TiO_2-coated samples.

Results in Figure 3b suggest the possibility that, at high O_2 partial pressures (i.e., >0.5 μmol), only a pseudo-saturation occurs, with the GPC increasing slightly beyond 0.5 Å/cycle with increasing pressure. The absence of definitive saturation is likely a result of the methodology used to control the O_2 dose in this case. Rather than varying the pulse time under fixed flow conductance, which is a more common technique, higher oxidant doses were achieved by increasing the O_2 flow rate and, thus, partial pressure for a fixed O_2 pulse time. Under such conditions, it has been reported that a higher conversion of the surface sites caused by the higher partial pressure of the oxidant can be achieved, leading to a higher GPC.[36,37] Based on the data from Figure 3b, optimized exposure conditions for O_2 correspond to ~0.8 μmol (or a pressure pulse of 1.2 Torr).

Although not the goal of this work, we note that, by increasing the O_2 partial pressure during the reaction, it was possible to grow RuO_2. Using a 10 Torr pulse of O_2 with an exposure time of 5 s (~12 μmol), the films became transparent and had a much higher resistivity of ~300 μΩ cm, as measured by four-point sheet resistivity probe, indicative of RuO_2. Ongoing research is aimed at understanding this transition and characterizing the films produced. Clearly, the onset of Ru oxidation reflects an upper limit on oxygen dose for a Ru ALD process.

As seen in Figure 4, the temperature process window for the Ru(C_9H_{13})$_2$−O_2 ALD Ru process was characterized by monitoring the GPC as a function of substrate temperature from 200 °C to 350 °C under optimized exposure and purge conditions (i.e. 2.2 and 0.8 μmol exposures for Ru(C_9H_{13})$_2$ and O_2 respectively, with 15 s purges between each). These data show a clear ALD process window between 250 °C and 300 °C, where the GPC remains constant at 0.5 Å/cycle. This represents an improvement over some of the more-common precursors. The sharp drop in the growth rate observed at temperatures above 300 °C (with zero growth at temperatures approaching 350 °C) most likely reflects a combination of thermal decomposition of the precursor, which is consistent with the DSC data shown in Figure 1b, and thermal desorption of the molecule from the substrate surface.

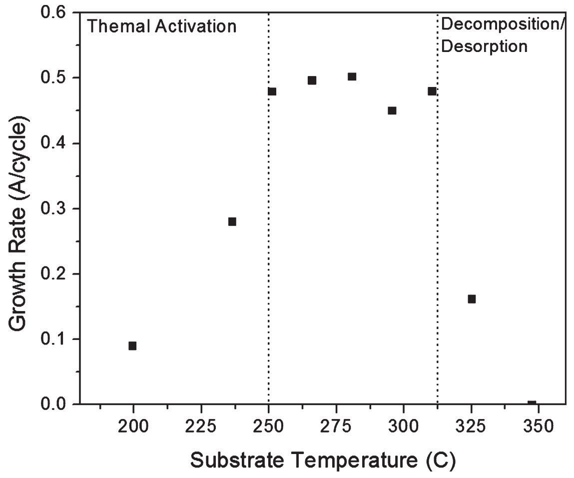

Figure 4. Temperature window showing the growth rate as a function of substrate temperature. A stable window is seen between 250 °C and ~312 °C. Beyond this temperature, some combination of precursor decomposition and thermal desorption from the substrate leads to a sharp decrease of the growth rate.

To investigate the nucleation kinetics of this Ru ALD process, we carried out the optimized ALD process on TiO_2- and Al_2O_3-coated surfaces, as well as on the SiO_2 and H-terminated Si surfaces. All of the substrates were held at 270 °C, which is well within the temperature window shown in Figure 4, and Ru films were deposited for 50, 100, 250, and 500 cycles. As can be seen in Figure 5, SiO_2 surfaces exhibit the shortest nucleation delays, followed by TiO_2 and, to a lesser degree, H-terminated Si. All of these substrates showed short nucleation delays, none larger than 50 cycles. Post-process ellipsometry measurements indicate a low (2%−5%) nonuniformity across the wafer. Four-point probe

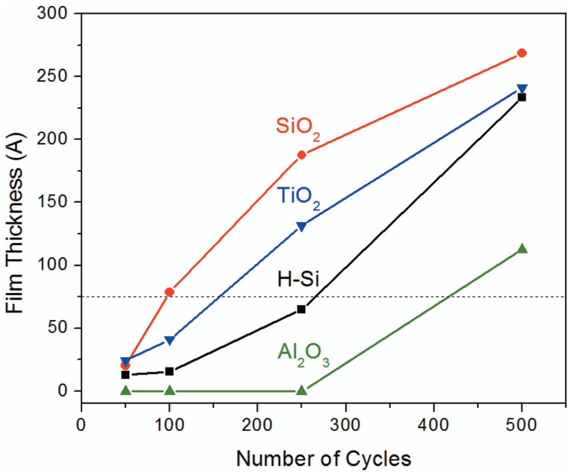

Figure 5. Film thickness as a function of total number of cycles for four different substrates, showing low nucleation retardation for SiO_2, TiO_2, and H-terminated Si. Data for Al_2O_3 shows a significantly higher nucleation barrier, requiring at least 250 cycles before film growth begins. Comparing film thickness data to XRD data shows that films less than ~75 Å thick (dotted line) are amorphous.

sheet resistance measurements of 25-nm Ru films indicate a resistivity of 20 $\mu\Omega$ cm.

Ru ALD deposition on Al_2O_3 reveals a significant nucleation delay, 250 cycles to initiate growth. As, presumably, all of the oxide materials involved surfaces are terminated with hydroxyl groups, we infer that the nucleation dynamics are not solely driven by the nature of the surface groups available for adsorption. It is noteworthy that nucleation on H-terminated Si is faster than that on the alumina surface. The peculiarities of Ru growth on these different substrates is discussed further below.

MATERIAL CHARACTERIZATION

Results from XRD (Figure 6) and SEM (Figure 7) show that the deposited films are nanograined polycrystalline films comparable to previously published results with Cp- and tris-β-diketonate-based chemistries.[25,27] Figure 6 shows the diffraction pattern for films deposited on four different substrates—SiO_2, TiO_2, H-terminated Si, and Al_2O_3—at three different thicknesses (except for Al_2O_3, which was only measured at 500 cycles (or ~100 Å)). Results for these data are reported in terms of the number of cycles rather than thickness, because of differences in thickness from slow or delayed nucleation. The observed diffraction peaks for Ru(100), Ru(002), Ru(101), and Ru(102), with Ru(102) only being seen on SiO_2 and TiO_2, appear comparable to other published results.[21,25−27,38] Peak intensities are dependent on the overall film thickness rather than on the nature of the substrate.

Films grown on SiO_2, TiO_2, and Si only show crystallinity at thicknesses over ~75 Å, as can be seen by comparing the results shown in Figure 5 to the XRD data shown in Figure 6. XRD for the Al_2O_3 substrates was only performed for 500 cycles, since nucleation was strongly delayed in this case (Figure 5), leading to low Ru coverage for smaller number of cycles (see SEM results below). Using the Debye−Scherrer equation, the average grain size over all orientations, except the (102), was calculated for each of the substrates, giving the following values: on Si, 13.11 ± 0.49 nm; on SiO_2, 16.57 ± 2.65 nm; on TiO_2, 16.49 ± 0.88 nm; and on Al_2O_3, 9.81 ± 1.24 nm.

SEM images for ALD Ru on the four substrates at 100, 250, and 500 cycles are shown in Figure 7, corresponding to the conditions for the XRD results in Figure 6. These images are consistent with the average grain size for the four cases as calculated by the Debye−Scherrer equation.

DISCUSSION

The issue of nucleation kinetics is particularly important in ALD, since ALD applications typically involve ultrathin layers, whether for semiconductor gate insulators or for novel nanostructures.[39] In other words, the thickness regime of ~1−50 nm is of prime interest for ALD; yet, some ALD surface chemistries (as shown here and elsewhere) may involve nucleation regimes covering much of this thickness regime. When that occurs, the benefit of ALD's thickness control is sharply degraded in that counting ALD cycles does not predict and control the ALD layer thickness, unless real-time diagnostics and metrology can be employed.[7] For the Ru ALD precursor and process reported here, nucleation kinetics is highly differentiated by the nature of the substrate surface, with favorable results for SiO_2 and TiO_2 surfaces, versus very unfavorable results for the Al_2O_3 surface.

A striking example of the consequences of this can be envisioned for the case of deposition into very-high-aspect-ratio nanopores.[39] One approach to nanostructures for energy applications is to build nanowire or nanotube devices initially within anodic aluminum oxide nanopores, using the conformality of ALD to do so. With such structures, thickness (and conformality) control are essential. The ALD Ru chemistry reported here nucleates very poorly on Al_2O_3. Since nucleation-controlled growth is often linked to varying defect sites on the surface, even the onset of nucleation may be variable. On the other hand, an ALD TiO_2 layer may be used to alter surface conditions on the anodic Al_2O_3 material prior to Ru ALD.

It is also important to note that there are differences in creating an optimal ALD process that allows uniform deposition over large surfaces areas (for example, a 4-in. wafer) and a process that allows conformal deposition over ultrahigh-aspect-ratio structures (for example, those created in porous anodic aluminum), although the two processes are clearly related chemically. Traditionally, ALD processes have been optimized over large flat areas (i.e., 4-in. wafers) by varying the components that make up the process space (such as metal−organic precursor dose, reactant dose, purge times, residence times, and substrate temperature), but which may also include reactor size and shape. Therefore, for the interests of this paper, we report cross-wafer uniformity and surface saturation as the ultimate measures of the ALD process. Future development of novel nanostructures will have to consider nucleation and uniformity (i.e., conformality) in high-aspect-ratio structures to be the more important measure of a successful process.

It is difficult to compare our nucleation results to that of previously published chemistries, because not all chemistries were studied using Al_2O_3. Furthermore, in those studies that did use Al_2O_3 as a substrate, $RuCp_2$, $Ru(thd)_3$, and $Ru(EtCp)_2$,[25,27,40] the lowest number of cycles used was 1000, and the data were then extrapolated back to determine the number of cycles that would presumably be required for nucleation. Such extrapolation is only valid if one assumes that, upon nucleation, a linear growth regime

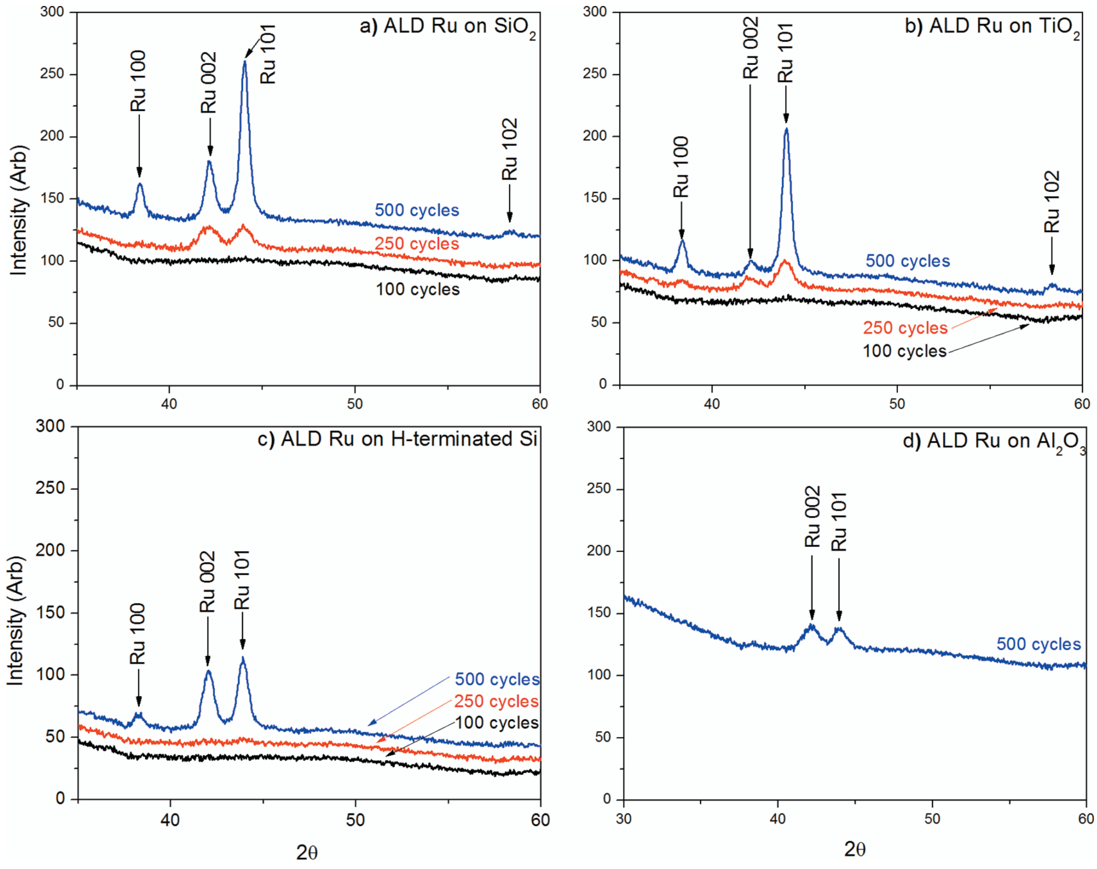

Figure 6. X-ray diffraction (XRD) data for films grown on four different substrates (as noted in top right corner of each panel). Films are all polycrystalline and show increased peak intensity as the thickness increases. Each substrate had three different thicknesses deposited on it, as noted by the number of cycles (blue corresponds to 500 cycles, red to 250 cycles, and black to 100 cycles).

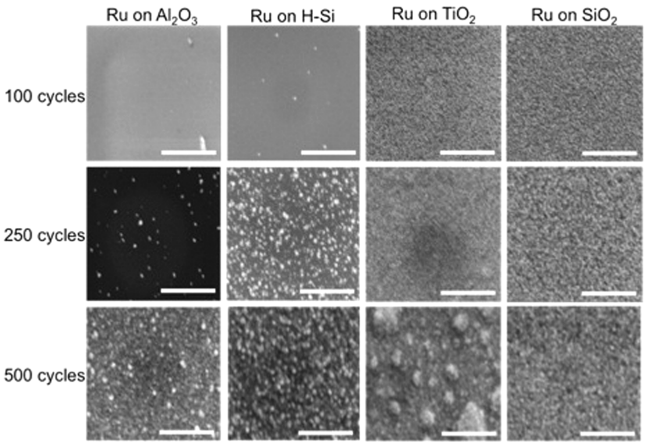

Figure 7. SEM images showing nucleation behavior of $Ru(C_9H_{13})_2$ on the four different substrates used: Al_2O_3, H-terminated Si, TiO_2, and SiO_2. Continuous films show a nanograin structure. Scale bar represents 500 nm.

with constant GPC is achieved. However, it has been shown that, in the case of three-dimensional island-type growth, a nonlinear growth regime is likely following nucleation, in which case extrapolating from a large number of cycles to a nucleation onset may lead to significant error in the estimation of nucleation delay.[41]

SEM images in Figure 7 for 500 cycles on TiO_2 indicate the formation of larger grainlike structures. As the XRD data shows a dominance of the (101) peak as the thickness of the Ru film is increased, we can assume that grains oriented in the (101) direction are emerging. A similar increased intensity for the (101) peak is seen on SiO_2 samples, although the difference between the (002) peak and the (100) peak are not as pronounced as they are on the TiO_2 samples, and the SiO_2 samples do not show the same large grain structures, despite the dominance of the (101) peak.

All of the substrates tested show a similar growth mechanism, which includes the formation of small island particles that eventually coalesces into a continuous film. These data suggest a growth mechanism controlled by island formation that follows the Volmer—Weber model.[35,42] Interestingly, the nucleation and growth behavior of the $Ru(C_9H_{13})_2$ precursor seems similar to that observed for $Ru(EtCp)_2$, where nucleation kinetics were shown to be strongly substrate-dependent and were primarily driven by island formation and coalescence mechanisms.[43] However, in our case, nucleation times on SiO_2 are significantly improved, because our data (see Figure 5) indicates that $Ru(C_9H_{13})_2$ involves little to no nucleation delay on SiO_2, compared to the reported 100—200 cycles delay for $Ru(EtCp)_2$.

As mentioned above, the XRD data in Figure 6 shows that the nucleation and growth behavior of the Ru film on H-terminated Si is significantly better than that on Al_2O_3. This conclusion is supported by the SEM data in Figure 7. However, Al_2O_3 should have the same terminations as SiO_2 and TiO_2 (i.e., the hydroxl groups accounted for in most models). Island growth models are dependent on the surface energy of the substrate and not solely on which surface groups are available, although these groups will presumably affect the surface energy. Recent studies where the surface energy of a substrate was modified showed that films could be forced to switch from monolayer growth to island growth, suggesting a far more complicated relationship between growth mechanism and substrate choice.[42]

Data presented here show that large differences in nucleation kinetics occur for this Ru ALD process and are most likely due to differences in surface energies, rather than on what surface species are available for bonding. This suggests that ALD—particularly with more-complex precursors—will require more intricate, fundamental modeling to explain some of the behavior reported in this paper.

■ CONCLUSIONS

A new precursor was developed specifically to address issues confronting the deposition of the noble metal ruthenium, including slow nucleation kinetics and undesirable precursor phases. The molecule developed—bis(2,6,6-trimethyl-cyclohexadienyl)ruthenium ($Ru(C_9H_{13})_2$)—was shown to have similar vapor pressure as commonly used Ru precursors such as RuCp and $Ru(EtCp)_2$, with superior thermal stability, as measured through thermogravimetric and DSC analysis.

As a precursor for the atomic layer deposition (ALD) of ruthenium, $Ru(C_9H_{13})_2$ exhibits self-limiting behavior as a function of organo-metallic precursor dosage, oxidant dosage, and substrate temperature. A temperature window was shown between 250 °C and 300 °C. Under suitable ALD surface saturation conditions, the GPC was shown to be 0.5 Å/cycle. Nucleation conditions on different substrates, including SiO_2, TiO_2, Al_2O_3, and H-terminated Si, showed significantly faster nucleation on SiO_2 and TiO_2, and, to a lesser extent, H-terminated Si, than on Al_2O_3, where large nucleation delays (on the order of 250 cycles) occur.

■ AUTHOR INFORMATION

Corresponding Author

*To whom correspondence should be addressed: rubloff@umd.edu.

Present Addresses

◆Cambridge Nanotech, Inc., 68 Rogers Street, Cambridge MA 02142, USA.

■ ACKNOWLEDGMENT

This material is based on work supported as part of the Science of Precision Multifunctional Nanostructures for Electrical Energy Storage, an Energy Frontier Research Center funded by the U.S. Department of Energy, Office of Science, Office of Basic Energy Sciences under Award Number DESC0001160. We acknowledge the support of the Maryland Nanocenter and its NISP lab. The NISP lab is supported in part by the NSF as a MRSEC shared experimental facility. Development of the precursor used in this paper was done exclusively by Air Liquide. Finally, the authors would like to thank Parag Banerjee for his insightful thoughts during the preparation of this manuscript.

■ REFERENCES

(1) George, S. M.; Ott, A. W.; Klaus, J. W. *J. Phys. Chem.* **1996**, *100* (31), 13121–13131.
(2) Knez, M.; Niesch, K.; Niinisto, L. *Adv. Mater.* **2007**, *19* (21), 3425–3438.
(3) Juppo, M.; *J. Vac. Sci. Technol. A* **1998**, *16* (5), 2845–2850.
(4) Klaus, J. W.; Ferro, S. J.; George, S. M. *Thin Solid Films* **2000**, *360* (1−2), 145–153.
(5) Elam, J. W.; *Surf. Sci.* **2001**, *479* (1−3), 121–135.
(6) Lei, W.; Henn-Lecordier, L.; Anderle, M.; Rubloff, G. W.; Barozzi, M.; Bersani, M. *J. Vac. Sci. Technol. B* **2006**, *24* (2), 780.
(7) Henn-Lecordier, L.; Lei, W.; Anderle, M.; Rubloff, G. W. *J. Vac. Sci. Technol. B* **2007**, *25* (1), 130.
(8) Martensson, P.; Carlsson, J. O. *J. Electrochem. Soc.* **1998**, *145* (8), 2926–2931.
(9) Lim, B. S.; Rahtu, A.; Gordon, R. G. *Nat. Mater.* **2003**, *2* (11), 749–754.
(10) Aaltonen, T.; *Chem. Mater.* **2003**, *15* (9), 1924–1928.
(11) Senkevich, J. J.; *Chem. Vapor Dep.* **2003**, *9* (5), 258–264.
(12) Ten Eyck, G. A.; *Chem. Vapor Dep.* **2005**, *11* (1), 60–66.
(13) Aaltonen, T.; Ritala, M.; Leskela, M. *Electrochem. Solid State Lett.* **2005**, *8* (8), C99–C101.
(14) Aaltonen, T.; *J. Electrochem. Soc.* **2004**, *151* (8), G489–G492.
(15) Hwang, C. *Mater. Sci. Eng. B* **1998**, *56*, 178.
(16) Choi, E. S.; Hwang, J. S.; Yoon, S. G. *J. Electrochem. Soc.* **2000**, *147* (6), 2340–2342.
(17) Bandaru, J.; Sands, T.; Tsakalakos, L. *J. Appl. Phys.* **1998**, *84* (2), 1121–1125.
(18) Aoyama, T.; *Jpn. J. Appl. Phys., Part 1* **1999**, *38* (4B), 2194–2199.
(19) Heinrich, B. *Can. J. Phys.* **2000**, *78* (3), 161–199.
(20) Misra, V.; Lucovsky, G.; Parsons, G. N. *MRS Bull.* **2002**, *27* (3), 212–216.
(21) Kwon, O. K.; *J. Electrochem. Soc.* **2004**, *151* (2), G109–G112.
(22) Moffat, T. P.; *J. Electrochem. Soc.* **2006**, *153* (1), C37–C50.
(23) Kim, W. H., . *Nanotechnology* **2008**, *19* (4), No. 045302.
(24) Kim, S. K.; *Adv. Mater.* **2008**, *20* (8), 1429.
(25) Aaltonen, T.; *Chem. Vapor Dep.* **2003**, *9* (1), 45–49.
(26) Kwon, O. K.; *Electrochem. Solid State Lett.* **2004**, *7* (4), C46–C48.
(27) Aaltonen, T.; *Chem. Vapor Dep.* **2004**, *10* (4), 215–219.
(28) Kim, S. K.; Hoffmann-Eifert, S.; Waser, R. *J. Phys. Chem. C* **2009**, *113* (26), 11329–11335.
(29) Min, Y. S.; *Adv. Mater.* **2003**, *15* (12), 1019.
(30) Eom, T.-K. *Electrochem. Solid-State Lett.* **2009**, *12* (11), D85–D88.
(31) Kirss, R. U. *Inorg. Chim. Acta* **2004**, *357* (11), 3181–3186.
(32) Cordes, J. F.; Schreiner, S. *Z. Anorg. Allg. Chem.* **1959**, *299* (1−2), 87–91.
(33) Shibutami, T.; *Electrochem. Solid State Lett.* **2003**, *6* (9), C117–C119.
(34) Kim, S. K.; *J. Electrochem. Soc.* **2007**, *154* (2), D95–D101.
(35) Middleman, S. Hochberg, A. K. *Process Engineering Analysis in Semiconductor Device Fabrication*; McGraw−Hill: New York, 1993.
(36) Matero, R.; *Thin Solid Films* **2000**, *368* (1), 1–7.
(37) Kuse, R.; *J. Appl. Phys.* **2003**, *94* (10), 6411–6416.
(38) Kukli, K.; *J. Electrochem. Soc.* **2010**, *157* (1), D35–D40.
(39) Banerjee, P.; *Nat. Nanotechnol.* **2009**, *4* (5), 292–296.
(40) Yim, S. S., . *Appl. Phys. Lett.* **2006**, *89* (9), No. 093115.
(41) Green, M. L.; *J. Appl. Phys.* **2002**, *92* (12), 7168–7174.
(42) Lee, J. P.; Jang, Y. J.; Sung, M. M. *Adv. Funct. Mater.* **2003**, *13* (11), 873–876.
(43) Yim, S. S. *J. Appl. Phys.* **2008**, *103* (11), No. 113509.